Robust entrainment of circadian oscillators requires specific phase response curves

Benjamin Pfeuty, Quentin Thommen, Marc Lefranc

Robust entrainment of circadian oscillators requires specific phase response curves

Benjamin Pfeuty
Laboratoire de Physique des Lasers, Atomes, et Molécules, CNRS, UMR8523
Interdisplinary Research Institute, CNRS, USR3078
Université Lille 1, F-59655 Villeneuve d'Ascq, France

Quentin Thommen
Laboratoire de Physique des Lasers, Atomes, et Molécules, CNRS, UMR8523
Interdisplinary Research Institute, CNRS, USR3078
Université Lille 1, F-59655 Villeneuve d'Ascq, France

Marc Lefranc
Laboratoire de Physique des Lasers, Atomes, et Molécules, CNRS, UMR8523
Interdisplinary Research Institute, CNRS, USR3078
Université Lille 1, F-59655 Villeneuve d'Ascq, France

Abstract

The circadian clocks keeping time of day in many living organisms rely on self-sustained biochemical oscillations which can be entrained by external cues, such as light, to the 24-hour cycle induced by Earth rotation. However, environmental cues are unreliable due to the variability of habitats, weather conditions or cue-sensing mechanisms among individuals. A tempting hypothesis is that circadian clocks have evolved so as to be robust to fluctuations in daylight or other cues when entrained by the day/night cycle.

To test this hypothesis, we analyze the synchronization behavior of weakly and periodically forced oscillators in terms of their phase response curve (PRC), which measures phase changes induced by a perturbation applied at different phases. We establish a general relationship between, on the one side, the robustness of key entrainment properties such as stability and phase shift and, on the other side, the shape of the PRC as characterized by a specific curvature or the existence of a dead zone. This result can be applied to computational models of circadian clocks where it accounts for the disparate robustness properties of various forcing schemes. Finally, the analysis of PRCs measured experimentally in several organisms strongly suggests a case of convergent evolution toward an optimal strategy for maintaining a clock that is accurate and robust to environmental fluctuations.

INTRODUCTION

Circadian entrainment is the process by which a biological clock with a period of approximately 24 hours is synchronized to environmental cycles associated with Earth rotation. A stable and precise phase relationship between internal and external times is vital for organisms that need to timely anticipate dawn or dusk in order to coordinate their physiology to diurnal environmental changes. For instance, a precise clock in phototrophic organisms like cyanobacteria or plants has been shown to optimize cell growth and fitness (1–3).

However, circadian clock precision is challenged by many sources of intrinsic and extrinsic variability, which could dramatically affect key properties of endogenous biochemical oscillations. A growing interest has therefore been devoted to investigate how the period and amplitude of these oscillations are impacted by genetic mutations (4, 5), molecular noise (6–9), or contextual variability (8, 10), which led to advocate the existence of design principles ensuring robust oscillatory behavior in circadian clocks (11–13).

Nevertheless, a robust endogenous clock does not guarantee by itself a precise phase relationship with the day-night cycle, since the environmental cues associated with the diurnal changes are also highly fluctuating. The daylight intensity and quality sensed by an organism depend on various environmental factors such as meteorological conditions, shade habitats or, for marine organisms, the distance to sea surface and water turbidity (14, 15). In addition, variations of the behavior and light-sensing abilities of individuals can also alter the light signal reaching their core molecular clock. Thus, individuals of the same species living in different places or times can experience a wide spectrum of light intensities over several orders of magnitude, raising the question of whether and how specific robustness strategies are implemented in their clock architectures to maintain a precise synchronization despite unreliable environmental cues. Although the importance of this problem was noted some time ago (16), the robustness of circadian clocks to daylight fluctuations and how this constraint shapes their molecular architecture have been little studied until very recently (17, 18). These computational studies have revealed disparate robustness capabilities depending on the clock model, which remains to be explained in a comprehensive approach.

A natural theoretical framework to address this issue is the dynamical system theory of synchronization (19, 20). In forced oscillatory systems, a phase-locked state specified by a stable phase shift between the external and the internal phases closely depends on forcing features such as amplitude, profile or period. Changing these forcing properties can alter the phase shift or induce complex dynamical regimes (e.g., quasi-periodic, period-doubled, or chaotic), which are both undesirable for a functional circadian clock. Thus, the question of whether a circadian clock is robust to daylight fluctuations can be generalized to the problem of how an oscillator can maintain a stable synchronization and phase relationship with a forcing cycle that exhibits significant variability. Assuming a weak forcing allows one to drastically simplify the theoretical analysis by utilizing perturbation theory in the vicinity of a periodic orbit (21–23), in which the infinitesimal phase response curve (IPRC) of a weakly coupled oscillator provides important information on its synchronization.

In this paper, we first lay out the theoretical approach within which two quantities measuring robustness of the entrained state with respect to forcing fluctuations are defined. The phase approximation in the weak forcing limit allows us to identify the geometric properties of phase response curves that contribute to the robustness and precision of the clock phase in presence of fluctuations in the forcing amplitude. The general criteria obtained are shown to explain and predict the robustness properties of biologically-based circadian models. Finally, the analysis of PRCs that have been measured experimentally in several organisms supports the idea that living organisms have evolved salient strategies to maintain an accurate clock that is robust to daylight fluctuations.

RESULTS

Circadian clock entrainment and phase approximation

The entrainment of circadian clocks by cyclic environmental changes is a paradigmatic example of an unidirectional synchronization process. A biochemical implementation of this process in a living cell involves a network of genes and proteins interacting with each other, whose temporal evolution is usually modeled by a set of ordinary differential equations:

$$\frac{d\mathbf{X}(\mathbf{t})}{dt} = \mathbf{F}(\mathbf{X}(t), \mathbf{p_0} + \mathbf{dp}(t)) \tag{1}$$

where the components of vector $\mathbf{X}$ are the concentrations of the molecular actors interacting according to the biochemical kinetics $\mathbf{F}$, derived from the law of mass action.

Synchronization of the circadian clock to the diurnal cycle requires that some parameters p_i are sensitive to temporal changes of light induced by the cycle, so that they differ from their value in the dark $(p_0)_i$ by

$$dp_i(t) = \epsilon\, L(u)\, v_i\, (p_0)_i \tag{2}$$

where the perceived light intensity is described by an amplitude ϵ and an a normalized temporal profile L which depends on $u = t - t_d$, with $u \in [0, T]$, t_d and T corresponding to dawn time and the 24-hour day length, respectively. The relative sensitivities of parameters to light are given by the vector $\mathbf{v}$, whose is normalized ($||\mathbf{v}|| = 1$) to ensure that ϵ is a relative modulation amplitude. In day/night entrainment conditions, the light sensed by the organism is assumed to be restricted to daytime of duration τ_D ($L(u) = 0$ for $u \in [\tau_D, T]$). In this work, an important point is that ϵ and L can differ between individuals depending on environmental or physiological context.

The existence of endogenous circadian oscillations requires that Eqs. 1 parameterized by $\mathbf{p}_0$ in the absence of light have an asymptotically stable limit cycle solution $\mathbf{X}_0$ characterized by a free-running period (FRP) T_0. The light-dependent perturbation deviates the circadian oscillator from its free limit cycle trajectory during daytime. If the amplitude deviation is not too large, the stability of the limit cycle ensures that the deviation decays in the absence of perturbation (during night), with the only memory of the past perturbation being a residual phase change. Thus, the Poincaré map of the dynamical system described by Eqs. 1 can be approximated by the following unidimensional map (11):

$$\phi_{n+1} = G(\phi_n) = \phi_n - \gamma + V(\phi_n, \epsilon) \tag{3}$$

where $\phi_n \in [0, T]$ is the oscillator phase in units of circadian hours (abbreviated as ch) (24) at which the light-dependent perturbation is switched on during the n-th day (i.e., the oscillator phase at dawn). $\gamma = (T_0 - T)T/T_0$ is the phase difference associated with the period mismatch between the forcing and endogenous periods. $V(\phi_n, \epsilon)$ is the phase change induced by the perturbation given by Eq. 2 applied at oscillator phase ϕ_n, and is known as a phase response curve (PRC) in the litterature (20). The mapping G has a stable fixed point if there exists a phase shift ϕ^* that satisfies:

$$\begin{cases} V(\phi^*, \epsilon) = \gamma \\ -2 < \partial_\phi V(\phi^*, \epsilon) < 0 \end{cases} \tag{4}$$

This phase-locked state is usually termed $1:1$ synchronization (or entrainment) state. The stability coefficient $\partial_\phi V(\phi^*, \epsilon)$ (also noted $V'(\phi^*)$) characterizes how fast fluctuations around ϕ^* decay.

Due to the transversal stability of the limit cycle and the neutral stability of the phase, one can assume that small perturbations mainly induce phase deviations, which comprehensively describe the

effect on oscillator dynamics. In the framework of the so-called phase approximation (22), the PRC $V(\phi)$ can then be derived from an impulse infinitesimal PRC (i-IPRC) $Z(u)$ according to a convolution integral, with the important property that it scales linearly with light stimulus amplitude (11):

$$V(\phi,\epsilon) = \epsilon \int_0^{\tau_D} Z(u+\phi)L(u)du = \epsilon\, W(\phi) \tag{5}$$

Besides the classic i-IPRC $Z(\phi)$, Eq. 5 also introduces the d-IPRC $W(\phi)$ that describes the phase response of the oscillator to day-like light perturbations of duration τ_D, temporal profile $L(u)$ and vanishingly small amplitude ϵ.

Two distinct metrics to measure clock entrainment robustness

The daylight intensities sensed by a living organism depend on environmental factors, habitat or cloud cover, which can vary in time and space. They can also vary due to the temporal or inter-individual variability of the light-sensing mechanism. To determine the impact of this variability on the clock precision, our approach is to investigate how the PRC $V(\phi)$ given by Eq. 3 reacts to changes of the daylight driving cycle, as recapitulated in Fig. 1. Indeed, changes in amplitude ϵ and temporal profile $L(u)$ modify the asymptotic entrainment state (Fig. 1 *A*), and the resulting variations in phase shift or stability coefficient can be determined from the associated changes in the PRC (Fig. 1 *B*).

To define relevant measures of robustness, we consider small changes of daylight intensities with respect to some average value:

$$\epsilon L(u) = \epsilon_0(L_0(u) + \delta\epsilon\tilde{L}(u)) \tag{6}$$

where $u \in [0,\tau_D]$, $\tilde{L}$ is an appropriately normalized perturbation profile and $\delta\epsilon$ is small compared to 1. Such a perturbation generally modifies the PRC $V(\phi,\epsilon)$, and consequently the phase shift ϕ^* and the stability coefficient $V'(\phi^*)$. Considering that these two important properties of entrainment should vary as little as possible, two complementary sensitivity measures Π and Σ can be defined, which are respectively the variance of the phase shift and the relative variance of the stability coefficient in response to small daylight fluctuations of randomly distributed amplitudes (see Appendix *A*). Assuming that the phase shift and stability coefficient depend linearly on amplitude perturbation $\delta\epsilon$, Π and Σ can be written:

$$\begin{cases} \Pi &= [D_{\delta\epsilon}\phi^*(\epsilon_0)]^2 \\ \Sigma &= [D_{\delta\epsilon}\partial_\phi V(\phi^*,\epsilon_0)/\partial_\phi V(\phi^*,\epsilon_0)]^2 \end{cases} \tag{7}$$

The quantity Σ provides indirect information about the entrainment range of the forcing mechanism. Indeed, there are usually minimum and maximum values of the forcing strength such that outside the interval they define, complex dynamical regimes such as quasiperiodic, period-doubled or chaotic ones occur (19). These alternative regimes are associated with a high variability of the phase shift, which is incompatible with the time-keeping function of the clock. Achieving stable entrainment for a large spectrum of daylight intensities therefore requires that the stability coefficient is sufficiently independent of forcing strength so that it does not approach marginal stability ($V'(\phi^*) = 0$ or -2) too closely. Even when the 1:1 entrainment state is stable over a wide range, the phase shift ϕ^* can still vary in presence of fluctuations of daylight amplitude and profile, which is measured by Π. It is important to emphasize that, because Π and Σ are defined in with respect to the asymptotic phase shift, this approach is restricted to the case where the relaxation time toward the asymptotic state is smaller that the correlation time of daylight fluctuations over successive days, for

instance when individuals are subjected to slow changes of weather, habitat, genotype or phenotype. This approach may nevertheless give reliable insights into the case where daylight intensities change from day to day.

Π and Σ sensitivities depend on the shape of IPRCs

The sensitivity measures defined by Eq. 7 characterize variations in phase shift and stability coefficients. These variations depend themselves on the response of the PRC $V(\phi)$ to small changes in the amplitude and temporal profile of the forcing scheme, which must be computed numerically or determined experimentally. In the limit of weak forcing, however, the PRC can be approximated as a mere convolution of Z with the forcing profile (see Eq. 5). Subsequently, Σ and Π can be expressed in a simple manner as a function of forcing amplitude ϵ, period mismatch γ and IPRC characteristics. In the following, we investigate the robustness with respect to two types of daylight fluctuations which may occur in nature, namely changes (i) in the daylight temporal profile or (ii) in the average daylight amplitude.

In the first case, the primary effect of the temporal profile changes in light signal is to produce phase-shift variability. Π can then be expressed as the function of $Z(\phi)$ (see Appendix *B*):

$$\Pi = \left[\frac{\int_0^{\tau_D} Z(u+\phi^*)\,\tilde{L}(u)\,du}{\int_0^{\tau_D} Z'(u+\phi^*)L_0(u)\,du} \right]^2 \tag{8}$$

Low values of Π are achieved by minimizing the ratio between the two integrals, which constraints function Z. The numerator of Π in Eq. 8 can be minimized for arbitrary light input profile fluctuations $\tilde{L}(u)$ when Z is constant over the coupling interval $[\phi^*, \phi^* + \tau_D]$, since $\int \tilde{L}(u)du = 0$. In contrast to this, maximizing the denominator of Π in Eq. 8 typically requires that Z decreases significantly over $[\phi^*, \phi^* + \tau_D]$. An optimal compromise between these two requirements is reached when the i-IPRC Z is constant on a large portion of the coupling interval except at the beginning and the end of the interval, where phase advances or delays occur, so that the dead zone slightly smaller than the coupling interval. To illustrate this point, Figs. 2A and 2C show two i-IPRCs computed for two different coupling schemes of the circadian model introduced in the following section. The IPRC in Fig. 2 *A* displays a large dead zone during daytime contrary to the one in Fig. 2 *C*. We will see later that this is associated with very different degrees of robustness of the two coupling mechanisms. Besides Π, quantities Π_k characterizing phase-shift variance with respect to sinusoidal fluctuations of random phases can also be defined (see Appendix *B*).

Considering now changes in average light intensity, their effect on phase shift variance is easily derived from the property that $V(\phi^*, \epsilon) = \gamma$ is constant, yielding $\Pi = [\gamma / V'(\phi^*)]^2$ (see appendix *B*). Entrainment stability is affected in a more subtle manner. We find that Σ can be expressed in terms of the d-IPRC function $W(\phi)$ and its derivatives (see Appendix *B*):

$$\Sigma = \left[1 - \frac{W(\phi^*)W''(\phi^*)}{W'(\phi^*)^2} \right]^2 \tag{9}$$

where ϕ^* satisfies $\epsilon W(\phi^*) = \gamma$. If the period mismatch γ or the second derivative $W''(\phi)$ are zero, $\Sigma = 1$. Lower (resp., larger) values of Σ associated with an extended (resp., reduced) stability domain of the entrainment state imply $\gamma W''(\phi^*) > 0$ (resp., < 0). Thus, robustness requires a convex PRC when FRP is larger than the forcing period, and a concave one in the opposite case. Again, Figs. 2 *B* and *D* show two d-IPRCs computed from the circadian model introduced in next section. The fact that their curvatures are opposite near CT0 suggests that they have different robustness properties,

as we will see later.

In this section, we have derived and discussed two simplified expressions for Π and Σ which are valid for fluctuations in daylight temporal profile and in average daylight intensities, respectively. This is because changes in the daylight temporal profile, unlike those in the average daylight intensities, tend to be uncorrelated over successive days, thus perturbing the phase-shift without destabilizing the entrainment state. For fluctuations in average daylight intensities, which may persist over several days or even be permanent (corresponding to differences between two individuals), destabilization is the most disrupting effect. In following sections, computation of Π (resp., Σ) will thus be carried using Eq. 8 (resp., Eq. 9) to characterize robustness to fluctuations in daylight temporal profile (resp., intensity).

Robustness to daylight fluctuations in a minimal model of circadian oscillator

The criteria derived above to ensure robust entrainment in the face of daylight fluctuations hold for any nonlinear oscillator subjected to weak enough forcing. In this section, we check whether these criteria also apply to a minimal circadian oscillator model where coupling to light is generally non-negligible, and for which the weak forcing approximation does not necessarily hold. In most organisms, endogenous clock oscillations appear to rely on a core negative feedback loop, through which a clock gene encodes proteins that activate (vs inactivate) its own transcriptional repressor (vs activator) (25). The presence of delays or nonlinearities along the loop favors the emergence of oscillations in this autoregulatory loop (26, 27). This basic clock architecture can be captured in low-dimensional dynamical models such as the one originally proposed by Leloup and Goldbeter for Neurospora clock (28): a gene sequence is transcribed into mRNA (M), which translates into a protein in the cytoplasm (P_c), further translocated in the nucleus (P_N) where it inactivates the gene:

$$\left\{\begin{array}{ll} \tau\frac{dM}{dt} & = s_M\frac{K_I^n}{K_I^n+P_N^n} - d_M\frac{M}{K_M+M} \\ \tau\frac{dP_C}{dt} & = s_P M - d_P\frac{P_C}{K_P+P_C} - k_1\,P_C + k_2\,P_N \\ \tau\frac{dP_N}{dt} & = k_1 P_C - k_2 P_N \end{array}\right. \tag{10}$$

The Michaelis-Menten-like kinetics used to describe transcription and degradation dynamics is required for the appearance of spontaneous oscillations. We use the following model parameters, which give rise to 24-hour oscillations in the dark: $n = 4$, $s_M = 2.2$, $K_I = 1.8$, $d_M = 0.84$, $K_M = 0.5$, $s_P = 0.4$, $d_P = 1.6$, $k_P = 0.13$, $k_1 = 0.4$, $k_2 = 0.45$, $\tau = 1$. The effect of light is to modify one or several parameters during a time interval τ_D and with gain ϵ as in Eq. 2. To investigate the influence of a mismatch between the forcing period T and the FRP T_0, the latter is varied by changing the time constant τ ($T_0 = 24\,\tau$).

To illustrate our analysis, we have selected two light-coupling schemes on the basis of their IPRCs so that they provide us with examples of robust and non robust entrainment with respect to daylight fluctuations. These two schemes consist in the activation or repression of transcription by light, corresponding respectively to an increase or a decrease of s_M during daytime. The IPRCs associated with transcriptional repression by light indicates an insensitivity during the time interval in which light is applied (Fig. 2 *A*) and a negative sign of the third derivative near its zero (Fig. 2 *B*). According to Eqs. 8 and 9, both properties are expected to favor entrainment robustness. The opposite conclusions hold for the IPRCs associated with transcriptional activation by light (Figs. 2 *C*, *D*), which presumably indicates poor robustness properties.

Fig. 3 confirms that these two forcing schemes significantly differ in the robustness of the entrainment state to variations in light intensity, as we anticipated from their IPRCs. In case of transcriptional repression by light, entrainment remains stable at various light levels (left panel of

Fig. 3 *A*), and the entrained oscillations vary little. In contrast to this, period doubling occurs when transcription is activated by light (right panel of Fig. 3 *A*).

As predicted by the theory, these different robustness properties of the two forcing schemes when light level changes for a given FRP can be traced back to how the PRC and its derivative change when light levels are increased (Fig. 3 *B*). In the case of transcriptional repression by light, the PRC varies very little in an extended neighborhood of the fixed point. In particular, $V'(\phi^*)$ remains well within the stability boundary, whereas in the case of transcriptional activation by light, the phase-locked state is destabilized ($V'(\phi^*) < -2$) beyond a critical forcing amplitude where period-doubling typically occurs (Fig. 3 *C*). Accordingly, values of Σ are much lower in the case of transcriptional repression by light at all forcing strengths (Fig. 3 *D*). Fig. 3 *E* shows that these robustness properties do not depend on the FRP. Whatever the value of the latter, the 1:1 entrainment domain is much wider for transcriptional repression by light. In fact, the main effect of the period mismatch is to force a minimum modulation amplitude for synchronization when it it increases or decreases away from 0.

These two light-coupling schemes are also associated with different robustness properties of the clock phase with respect to changes of the daylight temporal profile (Fig. 4). The phase shift variance induced by small sinusoid perturbations of different phases is much smaller (by a factor from 2 to 10) when light represses rather than activates the self-regulated gene (Fig. 4 *A*). Again, this difference in robustness can be explained by the sentitivity or insensitivity of the PRC near the stationary phase shift (Fig. 4 *B*), which ultimately depends on the existence of dead zone in the relevant time interval (Fig. 2 *A* and *C*). Fig. 4 *C* shows that these differences in phase-shift sensitivities with respect to sinusoidal profile fluctuations are more or less pronounced depending on the specific value of the FRP T_0, or of the characteristic period of the fluctuations ($k = 1$ or 2).

Taken together, Figs. 3 and 4 shows two light-coupling schemes that are associated with a large (resp. small) entrainment domain inside which there is a low (resp. large) phase-shift variability. In fact, the two quantities tend to be correlated, as is assessed by a systematic correlation analysis (see Fig. S1 in the Supporting Material).

Relating robustness to IPRC: validity of the weak coupling approximation

The extent to which IPRC properties can account for the robustness of circadian clock with respect to daylight fluctuations depends on the validity of the phase approximation. In this section, we therefore evaluate the agreement between robustness properties derived analytically in the limit of weak forcing and those measured numerically when the forcing is not weak, as depicted in Fig. 5.

A first indication is provided by estimating the light-stimulus amplitude beyond which the proportional relationship between phase response and light amplitude (Eq. 5) no longer holds. In this respect, we found that the phase approximation can remain acceptable for modulations in excess 50%, depending on the parameter considered and on the stimulus phase (Fig. 5 *A*, *B*). Other quantities derived from PRCs, like the phase shift ϕ^*, the stability coefficient $V'(\phi^*)$, or the phase-shift and coefficient stability sensitivities Π and Σ, are also expected to deviate from their estimates in the phase approximation. Estimation of the phase shift and the stability coefficient of the entrainment state is quantitatively good when parameters change by 30% between night and day (Fig. 5 *C*, *D*). Quantitative agreement is slightly more difficult for Π and Σ (Fig. 5 *E*, *F*), but a qualitative agreement can still be observed and is in fact more than sufficient to reflect a large (over 20-fold) dispersion of values of Π and Σ between the most and least robust entrainment schemes.

The study of the range of validity of our approach has been extended to more realistic circadian clock models associated with various organisms like Drosophila (28), Ostreococcus (18), cyanobacteria

(29) or mammals (30) (see Fig. S2 in the Supporting Material). The good agreement observed between robustness measures and their estimates using IPRC confirms that the phase approximation remains qualitatively valid for moderate forcing strength regardless of the model properties, thus providing an efficient tool to discriminate forcing schemes according to their robustness properties.

Experimental PRCs analysis reveal robustness properties to daylight fluctuations

We have shown that PRCs, despite of their simplicity, can provide a detailed and reliable information on the robustness properties of circadian entrainment. Incidentally, PRCs have been measured over fifty years in many organisms (31), thereby offering indirect evidence of whether natural clocks are robust or not to daylight fluctuations.

We have selected several PRCs measured in response to light pulses of various durations for twelve species (32–42) (Fig. 6 *A*). One may assume that for type-I experimental PRCs (a to j panels), the phase approximation holds. Therefore, their corresponding impulse IPRCs are expected to display a shape similar to that of experimental PRCs if the light pulse is short enough (panels *a*-*g* of Fig. 6 *A*) or can otherwise be obtained by a rectangular-pulse deconvolution (panels *h*-*j* of Fig. 6 *A*). In any case, the impulse IPRCs display pronounced dead zones (Fig. 6 *B*), albeit of different sizes, which is likely to confer robustness to daylight fluctuations according to our results.

For a quantitative assessment of this conjecture, we compare the values of Π for the i-IPRCs estimated from experimental data with those obtained for many different light-coupling schemes in various circadian models (Fig. 6 *C*). Values of Π obtained from experimental PRCs are found to be systematically lower than in the control case of a linear i-PRC, and are consistent with those computed for the most robust entrainment schemes of various circadian models. This strongly supports the idea that the circadian clock of these organisms have evolved robustness properties with respect to daylight fluctuations.

PRCs in response to daylight-like stimuli such as 12-hour rectangular pulse also provide valuable information about the entrainment robustness measured by the quantity Σ. Unfortunately, those PRCs have been much less measured experimentally, and can be hardly estimated from the PRCs available without a precise knowledge of the light-coupling profile. Noticeable exceptions are the PRCs measured in two species (41, 42) that are depicted in the panels (k) and (l) of Fig. 6 *A*. The apparent change of curvature from convex to concave when the circadian phase goes from negative to positive seems again to indicate a robust entrainment.

DISCUSSION

In most living organisms, a circadian clock synchronizes internal physiological processes with cyclic environmental changes (e.g, in light or temperature) associated with Earth rotation. A stable phase relationship between internal and external time is however challenged by cellular and environmental variability. Part of this variability is linked to the diurnal cycle, in particular fluctuations in daylight perceived. In this work, we have derived explicit criteria for the robustness of circadian entrainment to daylight variability. Combining analytical and numerical approaches, we have shown that robustness depends critically on the precise shape of the IPRC, which characterizes the linear response of an oscillator to vanishingly small light inputs. On the one hand, the existence of an extensive range of entrainment is favored by a convex (resp. concave) d-IPRC (IPRC for daily pattern of light) when the FRP is larger (resp. lower) than the day-night driving period. On the other hand, a low dispersion of the phase shift between the internal oscillator and the environmental driving cycle requires a phase

response insensitivity of the clock during daytime, the so-called dead zone, which is manifested by the null interval of the i-IPRC (IPRC for light impulse) during the subjective day.

These two PRC properties confering entrainment robustness to forcing fluctuations happen incidentally to be observed in circadian PRCs measured experimentally in many organisms, in particular the existence of a dead zone that seems to be universal. Although clock resetting toward a stable phase shift obviously requires that phase advances and delays in PRCs occur in early and late day respectively, the presence of a dead zone has apparently emerged as a strategy to avoid phase variability due to daylight fluctuations and to ensure entrainment stability. The different size of dead zone intervals observed in various species does not weaken the robustness hypothesis but rather suggests the existence of light-gating mechanisms that restrict the light sensitivity of the clock to a certain window of the day (18, 30). These universal PRC properties of circadian clock may reflect an universal strategy to minimize the impact of fluctuations in the forcing cycle on the clock phase, thus suggesting a convergent functional evolution of circadian clocks.

Trade-offs between multiple evolutionary goals

Circadian clock properties, including IPRC or FRP properties, are also constrained by other adaptive purposes besides the need for robustness to daylight fluctuations, raising the question of whether trade-offs are eventually required.

One important evolutive constraint for circadian clock is the requirement to achieve fast resetting after jetlag (43), which depends in first approximation on the derivative of the PRC at ϕ^* (optimal resetting is obtained for $V'(\phi^*) = -1$). For circadian oscillators that display a dead zone, the weak forcing approximation indicates that fast resetting requires that the dead zone must be slightly smaller than the daylight interval or/and that the FRP must be different from 24 hours. These two conditions are fully compatible with criteria for robustness to daylight fluctuations.

The variability of the FRP of the circadian rhythm is also a prevalent source of variability susceptible to affect clock phase (35). Daan and Pittendrigh stressed the fact that a clock characterized by (i) a FRP equal to 24 hours and (ii) a large dead zone of the PRC displays a phase instability for which a small change in the FRP causes a large change in phase shift. This result has been tempered by a modeling study (44) showing that entrained circadian oscillations for the Drosophila model, which also display a dead zone, have a wider range of stability when the FRP is close to 24 hours. These apparently contradictory results can be reconciled in the light of our results when reasoning in terms of d-IPRCs of the circadian oscillator and depending on whether one focus on the effect of the FRP variability on the destabilization of the 1:1 synchronization state or on the phase-shift dispersion. The argument of Daan and Pittendrigh relies on the assumption that the first derivative of the d-IPRCs is small (i.e., the dead zone of the i-IPRC is larger than the light-coupling interval) whereas the argument of Kurosawa and Golbeter depends primarily on the second derivative values of the d-IPRC. In fact, it is likely that any circadian oscillators is characterized by an optimal value of the FRP whose distance from 24 hours would achieve a compromise in maintaining phase-shift stability and precision in face of both sources of variability in daylight intensities and FRP.

Finally, seasonal variations of daylength is another environmental variation that the clock needs to adapt to by tracking dawn, dusk or both. Previous studies (30, 45) have shown that the presence of a dead zone is an efficient mechanism to achieve seasonal tracking of dawn (resp. dusk) with a FRP larger (resp. smaller) than 24 hours. However, this mechanism requires that the dead zone is larger than the light coupling interval for some short photoperiods, which may antagonize the requirement for a robust synchronization in presence of daylight fluctuations.

Thus, circadian clocks characterized by a dead zone during the subjective day and a finely tuned

FRP, eventually supplemented with specific light-gating mechanisms (18, 30), are suitable to achieve an efficient trade-off between multiple and unrelated evolutionary goals.

Toward design principles of circadian clocks

The concept of phase response curve was introduced and exploited to investigate theoretically and experimentally rhythmic and synchronization behaviors in various biological systems (20, 46). When oscillators are weakly perturbed, their PRC reduces to an infinitesimal analog whose linearity allows a more comprehensive analysis of the synchronization behavior (11, 22, 47). Applying this approach in the context of circadian clocks allowed us to characterize the robustness of circadian entrainment with respect to daylight fluctuations in terms of specific characteristics of infinitesimal PRCs. This finding opens up a broad range of issues regarding the biophysical implementation of specific phase response curve properties in circadian clocks, similarly to the role of ionic currents in shaping the phase response curve of neuronal oscillators (48, 49). So far, many features of oscillatory behavior have been related to the structural basis of the underlying biochemical oscillator (9, 26, 50–52), but not to phase response curve characteristics. Understanding how the phase response curve is shaped by various features of light coupling, including gating (30) and photo-adaptation (53), or intrinsic oscillator properties such as feedback, saturation or delays, would undoubtely shed light on the role of some key features of circadian clock designs across species.

Acknowledgment

The authors acknowledge support of from Agence Nationale de la Recherche (ANR) under reference 07BSYS004 and from CNRS through the Interdisciplinary Programme “Interface Physique-Chimie-Biologie: aide à la prise de risque”.

Appendices

Appendix A. General expression of robustness quantities

The first-return map in Eq. 3 approximates the dynamics of a periodically forced non-linear oscillator and introduces the function $V(\phi)$, namely a PRC, which is an implicit function of amplitude ϵ and temporal profile L of the light forcing. We consider first that forcing properties slightly vary among individuals with respect to some average daylight forcing $\epsilon_0 L_0(u)$:

$$\epsilon L(u) = \epsilon_0 (L_0(u) + \delta\epsilon\, \tilde{L}(u)) \tag{11}$$

where L (or L_0) is normalized with $1/\tau_D \int_0^{\tau_D} L(t)dt = 1$. This normalization must be preserved by an appropriate normalization of $\tilde{L}$ that depends on the type of fluctuations considered (appendix B).

We can now expand the phase shift ϕ^* and the stability coefficient $\partial_\phi V(\phi^*)$ up to first order in $\delta\epsilon$:

$$\left\{ \begin{array}{lcl} \phi^*(\epsilon_0, \delta\epsilon) & = & \phi^*(\epsilon_0, 0) + \delta\epsilon[D_{\delta\epsilon}\phi^*(\epsilon_0, 0)] + 0(\delta\epsilon^2) \\ \partial_\phi V(\phi^*, \epsilon_0, \delta\epsilon) & = & \partial_\phi V(\phi^*, \epsilon_0, 0) + \delta\epsilon[D_{\delta\epsilon}\partial_\phi V(\phi, \epsilon_0, 0)] + 0(\delta\epsilon^2) \end{array} \right. \tag{12}$$

We introduce the quantities Π and Σ defined as the relative variances of the phase shift and the stability coefficient induced by daylight fluctuation of random amplitude:

$$\left\{ \begin{array}{lcl} \Pi & = & \frac{<(\phi^*(\epsilon_0,\delta\epsilon)-\phi^*(\epsilon_0,0))^2>}{<\delta\epsilon^2>} \\ \Sigma & = & \frac{<(\partial_\phi V(\phi^*,\epsilon_0,\delta\epsilon)-\partial_\phi V(\phi^*,\epsilon_0,0))^2>}{<\delta\epsilon^2><\partial_\phi V(\phi^*,\epsilon_0,0)^2>} \end{array} \right. \tag{13}$$

The approximation of small fluctuation amplitudes in Eq. 12 allows to rewrite those quantities as following:

$$\left\{ \begin{array}{lcl} \Pi & = & [D_{\delta\epsilon}\phi^*(\epsilon_0, 0)]^2 \\ \Sigma & = & [D_{\delta\epsilon}\partial_\phi V(\phi^*, \epsilon_0, 0)/\partial_\phi V(\phi^*, \epsilon_0, 0)]^2 \end{array} \right. \tag{14}$$

According to the fixed point condition of the map (Eq. 3), $V(\phi^*(\delta\epsilon), \delta\epsilon) = V(\phi^*(0), 0) = \gamma$. Expanding $V(\phi^*, \delta\epsilon)$ up to first order in $\delta\epsilon$ leads to:

$$\partial_{\delta\epsilon} V(\phi^*, \epsilon_0, 0) + V(\phi^*, \epsilon_0, 0)\partial_{\delta\epsilon}\phi(\epsilon_0, 0) = 0 \tag{15}$$

Π can be therefore expressed uniquely as a function of the PRC, $V(\phi)$:

$$\Pi = \left[\frac{\partial_{\delta\epsilon} V(\phi^*, \epsilon_0, 0)}{\partial_\phi V(\phi^*, \epsilon_0, 0)} \right]^2 \tag{16}$$

Combining Eqs. 14 and 15 allows to develop the quantity Σ as follows:

$$\Sigma = \left[\frac{\partial_\phi \partial_{\delta\epsilon} V(\phi^*, \epsilon_0, 0)}{\partial_\phi V(\phi^*, \epsilon_0, 0)} - \frac{\partial_{\delta\epsilon} V(\phi^*, \epsilon_0, 0)\partial_\phi^2 V(\phi^*, \epsilon_0, 0)}{[\partial_\phi V(\phi^*, \epsilon_0, 0)]^2} \right]^2 \tag{17}$$

Appendix B. Approximation of robustness quantities in the weak forcing limit

Assuming that the forced periodic orbit remains in a close neighbourhood of the free-running periodic orbit, we can use the phase approximation, according to which:

$$V(\phi, \epsilon_0, \delta\epsilon) = \epsilon \left[W(\phi) + \delta\epsilon \, \tilde{W}(\phi) \right] \tag{18}$$

where

$$W(\phi) = \int_0^{\tau_D} L(u) Z(u+\phi) du \tag{19}$$

and

$$\tilde{W}(\phi) = \int_0^{\tau_D} \tilde{L}(u) Z(u+\phi) du \tag{20}$$

Substituting Eq. 18 in Eqs. 16 and 17 allows one to express the measures of robustness introduced above as functions of W and $\tilde{W}$:

$$\Pi = \left[\frac{\tilde{W}(\phi^*)}{W'(\phi^*)} \right]^2 \tag{21}$$

and

$$\Sigma = \left[1 - \frac{\tilde{W}(\phi^*) W''(\phi^*)}{W'(\phi^*)^2} \right]^2 \tag{22}$$

a. Fluctuations in the average daylight intensities

The simplest example of fluctuations in the light driving cycle corresponds to the case where the overall gain of the light signal fluctuates. The normalization requirement for $\tilde{L}(u)$ imposes that $\tilde{L}(u) = L(u)$ and $\tilde{W}(\phi) = W(\phi)$, which allows to rewrite the sensitivity quantities of Eqs. 21 and 22 as:

$$\Pi = \left[\frac{\gamma}{\epsilon W'(\phi^*)} \right]^2 \tag{23}$$

and

$$\Sigma = \left[1 - \frac{\gamma W''(\phi^*)}{\epsilon W'(\phi^*)^2} \right]^2 \tag{24}$$

b. Fluctuations in daylight profiles

Alternatively, one can also consider the case where only the temporal profile change with some normalized variance whereas the light intensity averaged over the day remains unchanged:

$$1/\tau_D \int_0^{\tau_D} \tilde{L}(u)^2 \, du = 1 \tag{25}$$

and

$$\int_0^{\tau_D} \tilde{L}(u) \, du = 0 \tag{26}$$

Note that this normalization of $\tilde{L}$ preserves the normalization of $L(u)$. Substituting Eqs. 19 and 20 in Eq. 21 allows us to rewrite Π as a function of Z instead of W:

$$\Pi = \left[\frac{\int_0^{\tau_D} Z(u+\phi^*)\,\tilde{L}(u)\,du}{\int_0^{\tau_D} Z'(u+\phi^*)L(u)\,du} \right]^2 \tag{27}$$

One can also estimate the phase-shift sensitivity in response to sinusoidal daylight fluctuations of period τ_D/k and phase ψ_k. Decomposing $\tilde{L}(u)$ as a Fourier series:

$$\tilde{L}(u,\psi) = \sum_k \tilde{l}_k cos(uk/\tau_D + \psi_k) \tag{28}$$

and substituting Eq. 28 in Eq. 27 leads to:

$$\Pi(\psi) = \left[\frac{\sum_k a_k\, cos(\psi_k) + b_k\, sin(\psi_k)}{\int_0^{\tau_D} Z'(u+\phi^*)L(u)\,du} \right]^2 \tag{29}$$

where a_k and b_k as the kth cosine and sine Fourier coefficients of the i-IPRC truncated on the subinterval in which daylight perturbs the clock (usually daytime). Summing over ψ_k between 0 and 2π gives the averaged phase shift associated with a arbitrary fluctuations of zero mean ($\delta l_0 = 0$) and unitary norm ($\sum_k \tilde{l}_k^2 = 1$):

$$\Pi =< \Pi(\psi) >_\psi = 1/2\pi \int_0^{2\pi} \Pi(\psi) d\psi = \sum_k \tilde{l}_k^2\, \Pi_k \tag{30}$$

where Π_k are the phase-shift variances associated with sinusoidal fluctuations of period τ_D/k :

$$\Pi_k = \frac{a_k^2 + b_k^2}{2\,W'(\phi^*)^2} \tag{31}$$

These quantities are for instance easily computed in the case where Z is a decreasing linear function on the interval of coupling, which leads to $\Pi_k = \tau_D^2/8\,k^2\,\pi^2$ for $L(u) = 1$ during daytime.

Appendix C. Robustness analysis of experimental PRCs

In this section, we briefly describe the procedure used to analyse the experimental PRCs. First, the fitting procedure adjusts the discrete experimental data t_j, y_j with $j = 1, N$ by a continuous function $f(t)$. It is based on the minimization of both the fitting error and the second derivative of f:

$$S_1 = \frac{k_1}{N} \sum_{j=1,N} (y_j - f(x_j))^2 + \frac{k_2}{T} \int_0^T [f''(t)]^2\, dt \tag{32}$$

The ratio k_2/k_1 is adjusted typically between 5 and 15 according to the data.

For experimental PRCs that are measured using relatively short light pulse of less than one hour, the estimated i-IPRC, z, is assumed to be roughly equal to f. Otherwise we perform a deconvolution operation to extract the estimated i-IPRCs, using a genetic algorithm to find the function, z, that

minimize the error quantity:

$$S_2 = \int_0^T \left[f(t) - \int_t^{t+\tau_D} z(u)du \right]^2 dt \tag{33}$$

To estimate Π-values associated with experimental PRCs, we use Eq. 31 with the estimated i-IPRCs z.

References

[1] Woelfle, W. A., Y. Ouyang, K. Phanvijhitsiri, and C. H. Johnson, 2004. The adaptive value of circadian clocks: An experimental assessment in cyanobacteria. *Curr. Biol.* 14:1481–1486.

[2] Dodd, A. N., N. Salathia, A. Hall, E. Kevei, R. Toth, F. Nagy, J. Hibberd, A. J. Millar, and A. A. Webb, 2005. Plant circadian clocks increase photosynthesis and growth and survival and and competitive advantage. *Science* 309:630–633.

[3] Graf, A., A. Schlereth, M. Stitt, and A. M. Smith, 2010. Circadian control of carbohydrate availability for growth in Arabidopsis plants at night. *Proc. Natl Acad. Sci. U S A.* 107:9458–9463.

[4] Price, J. L., J. Blau, A. Rothenfluh, M. Abodeely, B. Kloss, and M. Young, 1998. Double-time is a novel Drosophila clock gene that regulates PERIOD protein accumulation. *Cell* 94:83–95.

[5] Cheng, P., Y. Yang, and Y. Liu, 2001. Interlocked feedback loops contributes to the robustness of the neurospora circadian clock. *Proc. Natl Acad. Sci. U S A.* 98:7408–7413.

[6] Barkai, N., and S. Leibler, 2000. Biological rhythms: Circadian clocks limited by noise. *Nature* 403:267–268.

[7] Gonze, D., J. Halloy, and A. Goldbeter, 2002. Robustness of circadian rhythms with respect to molecular noise. *Proc. Natl Acad. Sci. U S A.* 99:673–678.

[8] Mihalcescu, I., W. Hsing, and S. Leibler, 2004. Resilient circadian oscillator revealed in individual cyanobacteria. *Nature* 430:81–85.

[9] Wang, J., L. Xu, and E. Wang, 2008. Robustness, dissipations and coherence of the oscillation of circadian clock: potential landscape and flux perspectives. *PMC Biophys.* 1:7.

[10] Dibner, C., D. Sage, M. Unser, C. Bauer, T. d'Eysmond, F. Naef, and U. Schibler, 2009. Circadian gene expression is resilient to large fluctuations in overall transcription rates. *EMBO* 28:123–134.

[11] Rand, D. A., B. V. Shulgin, D. Salazar, and A. J. Millar, 2004. Design principles underlying circadian clocks. *J. R. Soc. Interface* 1:119–130.

[12] Stelling, J., E. D. Gilles, and F. J. Doyle, 2004. Robustness properties of circadian clock architectures. *Proc. Natl Acad. Sci. U S A* 101:13210–13215.

[13] Wagner, A., 2005. Circuit topology and the evolution of robustness in two-gene circadian oscillators. *Proc. Natl Acad. Sci. U S A.* 102:11775–11780.

[14] Stramska, M., and T. D. Dicky, 1992. Variability of bio-optical properties of the upper ocean associated with diel cycles in phytoplankton population. *J. Geophys. Res.* 97:17873–17887.

[15] Graham, E. A., S. S. Mulkey, K. Kitajima, N. G. Phillips, and S. G. Wright, 2003. Cloud cover limits net CO2 uptake and growth of a rainforest tree during tropical rainy seasons. *Proc. Natl Acad. Sci. U S A.* 100:572–576.

[16] Beersma, D. G. M., S. Daan, and R. A. Hut, 1999. Accuracy of Circadian Entrainment under Fluctuating Light Conditions: Contributions of Phase and Period Responses. *J. Biol. Rhythms* 14:320–329.

[17] Troein, C., J. C. W. Locke, M. S. Turner, and A. J. Millar, 2009. Weather and Seasons Together Demand Complex Biological Clocks. *Current Biology* 19:1961–1964.

[18] Thommen, Q., B. Pfeuty, P. Morant, F. Correlou, F. Bouget, and M. Lefranc, 2010. Robustness of circadian clock to daylight fluctuations: hints from the picoeucaryote Ostreococcus tauri. *Plos Comput. Biol.* In press.

[19] Pikovsky, A., M. Rosenblum, and J. Kurths, 2000. Synchronization: A universal concept in nonlinear sciences. Cambridge University Press.

[20] Winfree, A. T., 2001. The Geometry of Biological Time. Springer Verlag, Berlin, 3rd edition.

[21] Winfree, A. T., 1967. Biological rhytms and the behavior of population of coupled oscillators. *J. theor. biol.* 16:15–42.

[22] Kuramoto, Y., 1984. Chemical Oscillations, Waves and Turbulence. New York: Springer.

[23] Kramer, M. A., H. Rabitz, and J. M. Calo, 1984. Sensitivity analysis of oscillatory systems. *Appl. Math. Modelling* 8:328–340.

[24] Pittendrigh, C. S., and D. H. Minis, 1964. The entrainment of circadian oscillations by light and their role as photoperiodic clocks. *Am. Nat.* 98:261–294.

[25] Young, M. W., and S. Kay, 2001. Time zones: a comparative genetics of circadian clocks. *Nature Genetics* 2:702–715.

[26] Novak, B., and J. Tyson, 2008. Design principles of biochemical oscillators. *Nat. Rev. Mol. Cell Biol.* 9:981–991.

[27] Morant, P. E., Q. Thommen, F. Lemaire, C. Vandermoere, B. Parent, and M. Lefranc, 2009. Oscillations in the Expression of a Self-Repressed Gene Induced by a Slow Transcriptional Dynamics. *Phys. Rev. Lett.* 102:068104.

[28] Leloup, J., D. Gonze, and A. Goldbeter, 1999. Limit cycle models for circadian rhythms based on transcriptional regulation in Drosophila and Neurospora. *J. Biol. Rhythms* 14:433–448.

[29] Rust, M. J., J. S. Markson, W. S. Lane, D. S. Fisher, and E. K. O'SheaK, 2007. Ordered phosphorylation governs oscillation of a three-protein circadian clock. *Science* 318:809–812.

[30] Geier, F., S. Becker-Weimann, A. Kramer, and H. Herzel, 2005. Entrainment in a Model of the Mammalian Circadian Oscillator. *J Biol Rhythms* 20:83–93.

[31] Johnson, C. H., 1990. Atlas of phase response curves for circadian and circadital rhythms, volume 4. Nashville, Tennessee: Department of Biology, Vanderbilt. University.

[32] Perlman, J., H. Nakashima, and J. F. Feldman, 1981. Assay and Characteristics of Circadian Rhythmicity in Liquid Cultures of Neurospora crassa. *Plant Physiol.* 67:404–407.

[33] Konopka, R. J., 1979. Genetic dissection of the Drosophila circadian system. *Fed Proc.* 38:2602–2605.

[34] Covington, M. F., S. Panda, X. L. Liu, C. A. Strayer, D. R. Wagner, and S. A. Kay, 2001. ELF3 modulates resetting of the circadian clock in Arabidopsis. *Cell* 13:1305–1315.

[35] Daan, S., and C. Pittendrigh, 1976. A functional analysis of circadian pacemakers in nocturnal rodents. II. The variability of phase response curves. *J. Comp. Physiol.* 106:253–266.

[36] Honma, K., S. Honma, and T. Hiroshige, 1985. Response curve and free-running period and and activity time in circadian locomotor rhythm of rats. *Jpn J. Physiol.* 35:643–658.

[37] Fuentes-Pardo, B., and J. Ramos-Carvajal, 1983. The phase response curve of electroretinographic circadian rhythm of crayfish. *Comp. Biochem. Physiol.* 74:711–714.

[38] Johnson, C. H., I. Miwa, T. Kondo, and J. W. Hastings, 1989. Circadian rhythm of photoaccumulation in Paramecium bursari. *J. Biol. Rhythms* 4:405–415.

[39] Christianson, R., and B. M. Sweeney, 1973. The dependence of the phase response curve for the luminescence rhythm in gonyaulax on the irradiance in constant conditions. *Int. J. Chronobiol.* 1:95–100.

[40] Eskin, A., 1971. Some properties of the system controlling the circadian activity rhythm of sparrows. *M Menaker, Editor, Biochronometry, National Academy of Sciences, Washington* 55–80.

[41] Saunders, D. S., 1978. An experimental and theoretical analysis of photoperiod induction in the flesh fly and Sarcophaga argyrostoma. *J. Comp. Physiol.* 124:75–95.

[42] Saunders, D. S., and E. Thomson, 1977. 'Strong' phase response curve for the circadian rhythm of locomotor activity in a cockroach (Nauphoeta cinerea). *Nature* 170:241–243.

[43] Granada, A., and H. Herzel, 2009. How to achieve fast entrainment: The timescale to synchronization. *PLoS ONE* 4:e7057.

[44] Kurosawa, G., and A. Goldbeter, 2006. Amplitude of circadian oscillations entrained by 24-h light-dark cycles. *J. Theor. Biol.* 242:478–488.

[45] Gunawan, R., and F. J. Doyle, 2007. Phase sensitivity analysis of circadian rhythm entrainment. *J. Biol. Rhythms* 22:180–194.

[46] Granada, A., R. M. Hennig, B. Ronacher, A. Kramer, and H. Herzel, 2009. Phase response curves elucidating the dynamics of coupled oscillators. *Methods Enzymol.* 454:1–27.

[47] Taylor, S. R., R. Gunawan, L. R. Petzold, and F. J. Doyle, 2008. Sensitivity Measures for Oscillating Systems: Application to Mammalian Circadian Gene Network. *IEEE Trans. Automat. Contr.* 19:177–188.

[48] Pfeuty, B., G. Mato, D. Golomb, and D. Hansel, 2003. Electrical synapses and synchrony: the role of intrinsic currents. *J. Neurosci.* 23:6280–6294.

[49] Acker, C. D., N. Kopell, and J. A. White, 2003. Synchronization of strongly coupled excitatory neurons: relating network behavior to biophysics. *J Comput Neurosci.* 15:71–90.

[50] Tsai, T. Y., Y. S. Choi, W. Ma, J. R. Pomerening, C. Tang, and J. E. F. Jr, 2008. Robust and tunable biological oscillations from interlinked positive and negative feedback loops. *Science* 321:126–129.

[51] Pfeuty, B., and K. Kaneko, 2009. The combination of positive and negative feedback loops confers exquisite flexibility to biochemical switches. *Phys. Biol.* 6:046013.

[52] Stricker, J., S. Cookson, M. Bennett, W. Mather, L. Tsimring, and J. Hasty, 2008. A fast, robust and tunable synthetic gene oscillator. *Nature* 456:516–519.

[53] Malzahn, E., S. Ciprianidis, K. Kaldi, T. Schafmeier, and M. Brunner, 2010. Photoadaptation in Neurospora by Competitive Interaction of Activating and Inhibitory LOV Domains. *Cell* 42:762–772.

Figure Legends

Figure 1.

Measures of clock robustness to daylight fluctuations. (*A*) Example of two distinct daylight profiles (*top panel*) leading to different phase shifts for the entrained oscillators (*bottom panel*). The shaded area corresponds to night. (*B*) In the top panel, plots of the PRCs $V(\phi)$ measuring the phase change induced by the daylight perturbations shown in A applied at different phases. The stable phase shifts ϕ^* in the entrainment regime are solutions of $V(\phi) = \gamma$ defining . Infinitesimal values of $\Delta\phi^*$ with respect to small forcing discrepancies defines the sensitivity measure Π. In the bottom panel, plot of the derivative of the two PRCs, from which the stability coefficients $V'(\phi^*)$ of the entrainment states and their difference can be inferred. The shaded area corresponds to stable entrainment, associated with $-2 < V'(\phi^*) < 0$. Infinitesimal values of $\Delta V'(\phi^*)$ with respect to small forcing discrepancies defines the sensitivity measure Σ.

Figure 2.

Two IPRCs associated with different robustness properties and their characteristics. Plots of IPRCs in a circadian model where light induces either a repression (*A*,*B*) or an activation (*C*,*D*) of clock gene transcription. In these examples, FRP is 24 hours ($\gamma = 0$). (*A*,*C*) Plot of i-IPRCs $Z(\phi)$ measured in response to light impulses. Whether or not they display a dead zone during the light-coupling interval (*full line*) determines the phase-shift sensitivity Π to daylight fluctuations according to the Eq. 8. (*B*,*D*) Plots of d-IPRCs $W(\phi)$ measured in response to 12-hour rectangular light pulses. Slight changes of γ modify the entrainment phase shift ϕ^* (that would correspond to a displacement along the *full line* of W). Whether or not the $W''(\phi^*) > 0$ (resp., < 0) (*inset panel*) when $W(\phi^*) > 0$ (resp., < 0) determines the sensitivity Σ of the entrainment stability to daylight fluctuations according to the Eq. 9.

Figure 3.

Range of stable 1:1 entrainment in the face of light-amplitude fluctuations (*A*) Time course over one day of the M clock component (*full lines*) for different light forcing amplitudes (green: $\epsilon = 0.3$; red: $\epsilon = 0.6$; blue: $\epsilon = 0.9$) which modulate negatively (*left panel*) or positively (*right panel*) s_M (*dashed line*). The shaded area corresponds to night. The FRP is set to $T_0 = 25$ hours. (*B*) Plots of $V(\phi)$ and $V'(\phi)$ corresponding to the different forcing strengths shown in (*A*) (*same color code*). The shaded area corresponds to a stable 1:1 entrainment state. (*C*,*D*) Plots of $V'(\phi^*)$ and Σ as a function of ϵ for $T_0 = 25$ hours. (*E*) Phase diagram showing the different dynamical regimes that can be observed as a function of the forcing amplitude ϵ and period mismatch γ, extrapolated from the existence of a stable phase shift ϕ^* and the value of $V'(\phi^*)$ (1:1 Sync: 1:1 entrainment, $-2 < V'(\phi^*) < 0$; QP : quasi-periodicity, $V(\phi^*) = \gamma$ has no solution ; CS : complex synchronization and chaos, $V'(\phi^*) < -2$).

Figure 4.

Sensitivity of phase-shift to light-profile fluctuations. Left and right panels correspond to negative and positive modulation of s_M by light during daytime with $\epsilon = 0.3$. (*A*) Time courses of the light-dependent parameter and of the entrained circadian oscillations over one day in presence of sinusoidal daylight fluctuations. The FRP T_0 is set to 24 hours. (*B*) Changes in PRCs associated

wit fluctuations shown in A. The thick red lines indicate the range of phase shifts ($\gamma = 0$). (*C*) Corresponding values of $\Pi_k^{1/2}$ as a function of γ (*full line*: $k = 1$; *dashed line*: $k = 2$).

Figure 5.

Validity of the weak forcing approximation. (*A*, *B*) Plot of normalized PRCs $V(\phi)/\epsilon$ for various forcing strengths ranging from $\epsilon = 0.05$ (*black line*) to $\epsilon = 0.5$ (*red line*). In the presence of light, s_M decreases in A and increases in B. (*C-F*) Plots of various measures of synchronization and their estimates using IPRCs computed for all possible one-parameter modulations, with a light-modulation strength of $\epsilon = 0.3$ and FRP of $T_0 = 23.7$ and 24.3 hours. (*C*) Phase shifts ϕ^*. (*D*) Stability coefficient $V'(\phi^*)$. (*E*,*F*) Square roots of Σ and Π. Dashed lines correspond to the control case of an IPRC linearly decreasing during the daylight interval.

Figure 6.

Experimental PRCs reveal robustness properties. (*A*) Experimental PRC data (*triangles*) collected from many organisms (31) and fitted (*full line* and *shaded area*) according to the procedure described in the Appendix *C*. (*a*) Drosophila melanogaster, 40 min pulse (33); (*b*) Rattus albicus, 30 min pulse (36); (*c*) Mus musculus, 15 min pulse (35); (*d*) Mesocricetus Auratus, 15 min pulse (35); (*e*) Neuropora crassa, 5 min pulse (32); (*f*) Arabidopsis Thaliana, 1 hour pulse (34); (*g*) Procambarus bouvieri, 15 min pulse (37); (*h*) Passer domesticus, 6 hour pulse (40); (*i*) Gonyaulax polyedra, 3 hour pulse (39); (*j*) Paramecium Bursaria, 4 hour pulse (38) (*k*) Nauphoeta cinerea, 12 hours pulse (42); (*l*) Sarcophaga argyrostoma, 12 hour pulse (41). (*B*) Estimated i-IPRCs associated from the fitted data of the panel (*a*) to (*j*) of (*A*). (*C*) Plots of the ranges of $\Pi_{k=1}^{1/2}$-values (*a-j*, *shaded area*) computed from estimated i-IPRCs shown in (*B*) related with data shown in (*A*) associated with some range of FRP around 24 hours. For comparison, plots of the ranges of $\Pi_{k=1}^{1/2}$-values (*k*, *shaded area*) computed for all coupling schemes of the computational circadian clock model (see Fig. 5 *F*). The horizontal solid line indicates the value obtained for a linear IPRC (i.e., with zero curvature).

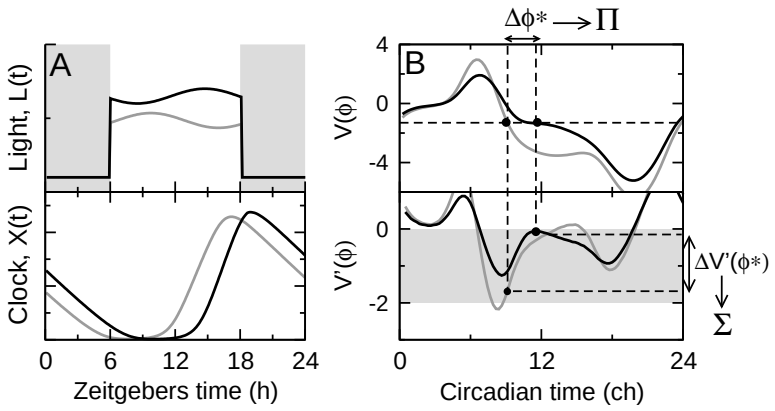
A
Light, L(t)
Clock, X(t)
0
6
12
18
24
Zeitgebers time (h)
Δϕ* ⟶ Π
B
V(ϕ)
V'(ϕ)
4
0
-4
0
-2
ΔV'(ϕ*)
Σ
0
12
24
Circadian time (ch)

Figure 1:

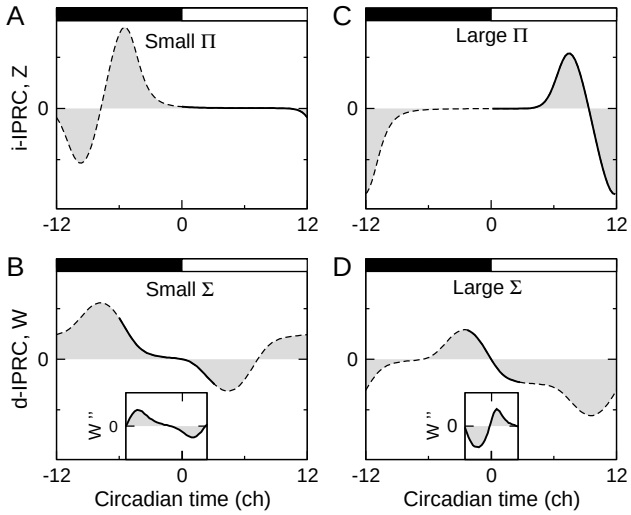
A
Small Π
i-IPRC, Z
0
-12
0
12
C
Large Π
0
-12
0
12
B
Small Σ
d-IPRC, W
0
W ''
0
-12
0
12
Circadian time (ch)
D
Large Σ
0
W ''
0
-12
0
12
Circadian time (ch)

Figure 2:

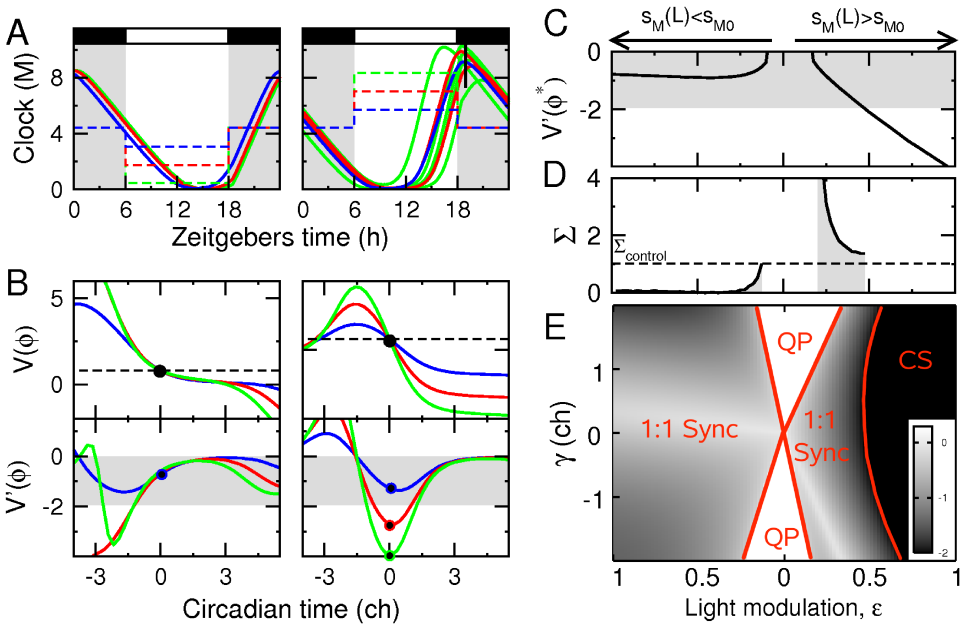
A
Clock (M)
8
4
0
0 6 12 18
0 6 12 18
Zeitgebers time (h)
B
V(ϕ)
5
0
V'(ϕ)
0
-2
-3 0 3
-3 0 3
Circadian time (ch)
C
s_M(L)<s_M0
s_M(L)>s_M0
V'(ϕ*)
0
-2
D
Σ
4
2
0
Σ_control
E
γ (ch)
1
0
-1
QP
CS
1:1 Sync
1:1 Sync
QP
1 0.5 0 0.5 1
Light modulation, ε

Figure 3:

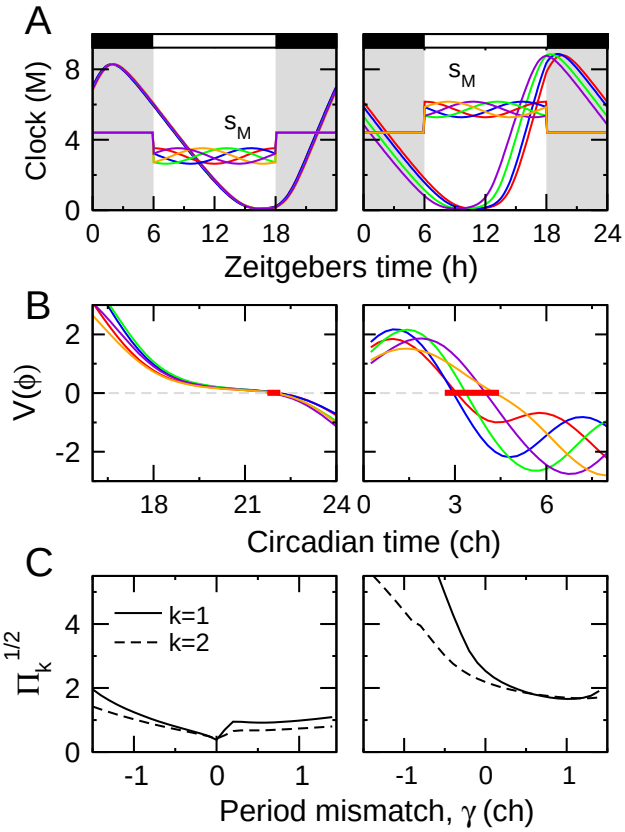
A
Clock (M)
8
4
0
s_M
s_M
0 6 12 18 0 6 12 18 24
Zeitgebers time (h)
B
V(ϕ)
2
0
-2
18 21 24 0 3 6
Circadian time (ch)
C
$\Pi_k^{1/2}$
4
2
0
k=1
k=2
-1 0 1 -1 0 1
Period mismatch, γ (ch)

Figure 4:

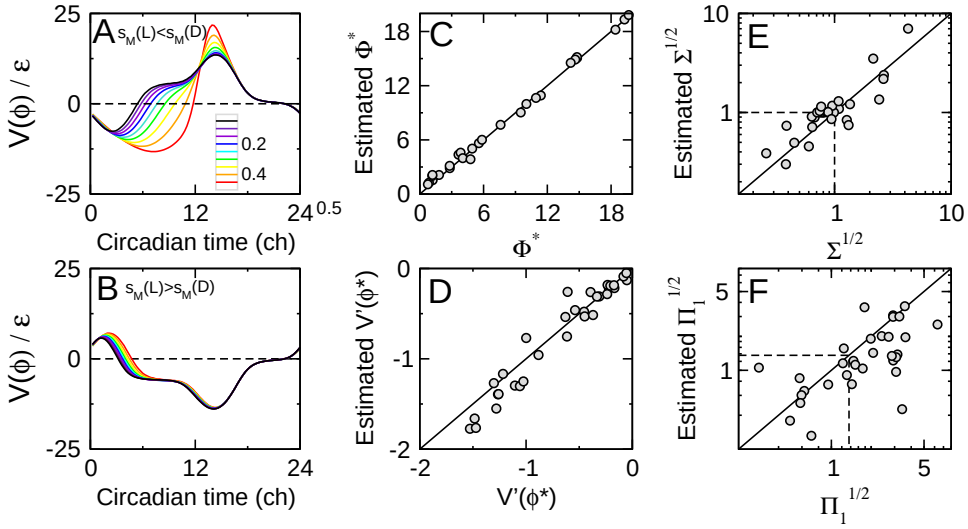
A
$s_M(L)<s_M(D)$
B
$s_M(L)>s_M(D)$
V(ϕ) / ε
Circadian time (ch)
0.2
0.4
0.5
C
D
E
F
Estimated Φ*
Φ*
Estimated V'(ϕ*)
V'(ϕ*)
Estimated Σ^1/2
Σ^1/2
Estimated Π_1^1/2
Π_1^1/2

Figure 5:

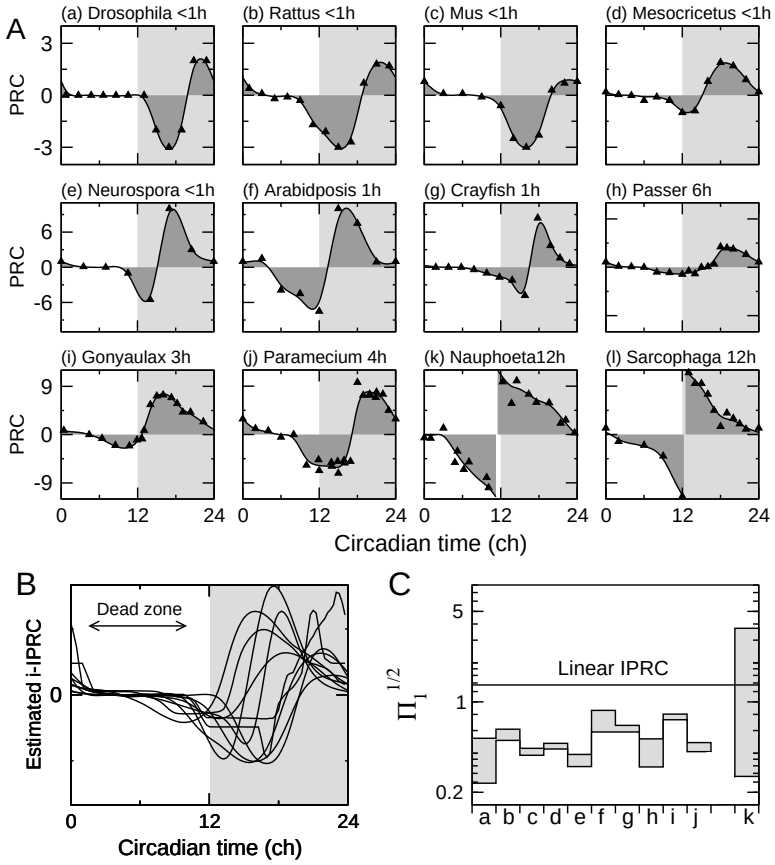
A
(a) Drosophila <1h
(b) Rattus <1h
(c) Mus <1h
(d) Mesocricetus <1h
(e) Neurospora <1h
(f) Arabidposis 1h
(g) Crayfish 1h
(h) Passer 6h
(i) Gonyaulax 3h
(j) Paramecium 4h
(k) Nauphoeta12h
(l) Sarcophaga 12h
PRC
Circadian time (ch)
B
Dead zone
Estimated i-IPRC
Circadian time (ch)
C
Linear IPRC
a b c d e f g h i j k

Figure 6: